Coulomb and nuclear effects in direct breakup of 54-MeV ^{7}Li + ^{12}C, ^{197}Au

J. E. Mason, S. B. Gazes, R. B. Roberts, and S. G. Teichmann
Nuclear Structure Research Laboratory, University of Rochester, Rochester, New York 14627
(Received 18 February 1992)

Direct breakup of $^{7}\mathrm{Li} \rightarrow \alpha + t$ was measured for 54-MeV ^{7}Li + ^{12}C, ^{197}Au reactions. The breakup products were detected in coincidence using a close-geometry detection system, and small scattering angles, forward of grazing, were investigated. The direct-breakup cross sections for $^{12}\mathrm{C}(^{7}\mathrm{Li},\alpha t)^{12}\mathrm{C}_{g.s.}$ exhibit significant enhancements beyond predictions of simple $E1$ Coulomb-breakup calculations, indicating the importance of the nuclear field. Direct-breakup yields in $^{197}\mathrm{Au}(^{7}\mathrm{Li},\alpha t)$ quasielastic reactions are sensitive to detector geometry, with the asymptotic fragment energies exhibiting target-proximity effects. Three-body classical trajectory calculations are found to provide qualitative agreement with these observations, provided the projectile is treated as an extended object. These strong Coulomb and nuclear effects severely complicate the extraction of radiative-capture cross sections and low-energy astrophysical S factors.

PACS number(s): 25.70.Mn, 95.30.Cq

I. INTRODUCTION

The breakup of $^{7}\mathrm{Li} \rightarrow \alpha + t$ is of current interest [1–8]. By detecting the breakup fragments in a coincidence measurement, information can be obtained about the underlying reaction mechanism. The breakup reactions observed are of two types: sequential breakup, a two-step process in which the ^{7}Li is first excited to a discrete state and then decays in flight, and direct breakup, in which breakup occurs as the rapid fragmentation of ^{7}Li without proceeding through an intermediate state.

Sequential and direct components in elastic breakup of ^{7}Li were first observed and unambiguously identified by Shotter *et al.* [1,2]. In those experiments, direct breakup was clearly observed only in reactions with high-Z targets such as ^{208}Pb [1] and ^{120}Sn [2]. No significant direct-breakup yield was measured for reactions on ^{12}C [1]. A dependence of direct-breakup yield upon target Z suggests that the Coulomb force may dominate the direct-breakup process. However the difficulty in probing very small scattering angles can also be responsible for this apparent Z dependence.

Recent theoretical studies [9, 10] have suggested that direct Coulomb-breakup cross sections can be used to gain information on the time-reversed process of radiative capture, using detailed balance. Since radiative-capture experiments are very difficult to carry out at astrophysically interesting energies due to sharply falling yields and associated experimental limitations, the use of direct Coulomb-breakup measurements has been proposed as a way of determining the reaction rates at these low energies. Provided that no nuclear or higher-order Coulomb effects contribute to the reaction, astrophysical S factors can be extracted for low relative energies. Recently, α-t relative kinetic energies from ^{7}Li breakup have been measured down to 34 keV, using a spectrograph to detect both fragments [3, 4]. In that work, it was argued that nuclear and final-state Coulomb interactions could be neglected in extracting a relative-energy distribution from the direct-breakup yield.

In this paper, we report on the elastic breakup of 54-MeV ^{7}Li on ^{12}C and ^{197}Au targets to further explore the Z dependence of the direct-breakup yield. The experimental fragment energy spectra and direct-breakup angular distributions are compared to results from three-body classical-trajectory calculations and Coulomb-breakup calculations, respectively. Special attention is given to the effects of detector orientation. We observe strong nuclear and Coulomb effects which are found to severely complicate the extraction of radiative-capture cross sections and, hence, astrophysical S factors. Some of the results reported here have been discussed previously [11].

II. BREAKUP KINEMATICS

The reaction kinematics of ^{7}Li breakup are illustrated in Fig. 1. The primary ^{7}Li is emitted with a velocity $\mathbf{v}_{\mathrm{lab}}$ and angle θ_{lab}. The alpha particle and triton are then emitted with velocities $\mathbf{v}_{\alpha}$ and $\mathbf{v}_{t}$ at angles θ_{α} and θ_{t}, respectively, in the laboratory reference frame. Sequential breakup from a particle-unstable state in ^{7}Li results in a well-defined relative kinetic energy of

$$E_{\mathrm{rel}} = E^{*} - E_{\mathrm{sep}},$$

where E^{*} is the energy of the excited state in ^{7}Li and

$$E_{\mathrm{sep}} = (m_{\alpha} + m_{t} - m_{\mathrm{Li}})c^{2} = 2.47 \text{ MeV}$$

is the separation energy for alpha-triton dissociation. For a fixed relative energy, the alpha particles and tritons are emitted such that their relative velocities, $\mathbf{v}_{\mathrm{rel}}$, define "breakup spheres" centered on the primary ^{7}Li.

A coincidence-detection system (represented in Fig. 1 by the solid angles $\Delta\Omega_{\alpha}$ and $\Delta\Omega_{t}$ of alpha particle and

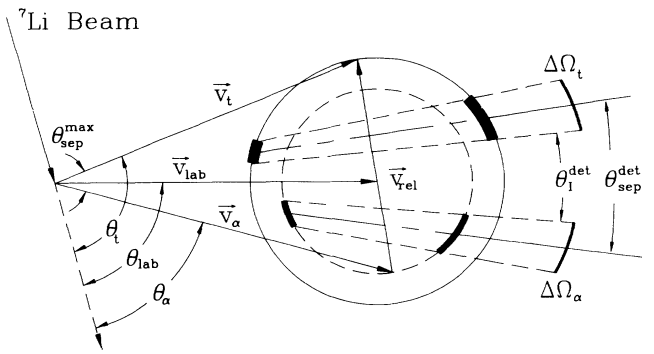

FIG. 1. Schematic of the breakup kinematics for $^7\text{Li} \rightarrow \alpha + t$. Laboratory velocities and angles are shown. The center-to-center separation angle of the detectors is θ_{sep}^{det} while the smallest alpha-triton separation angle for a detectable coincidence is θ_I^{det}. Laboratory solid angles of the detectors and their intersection with the breakup spheres are also indicated.

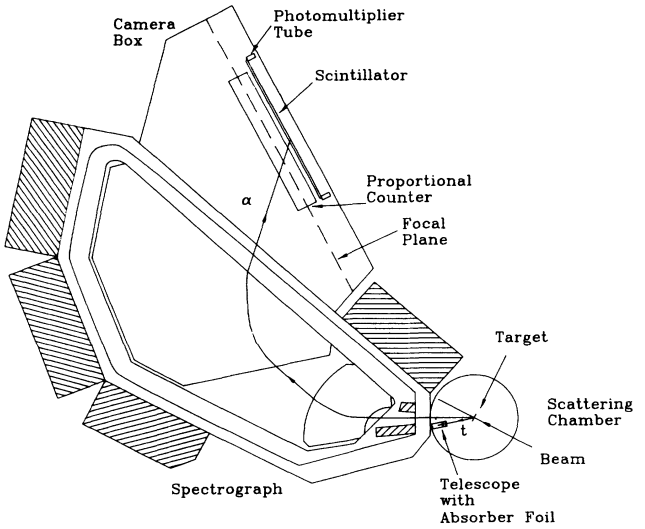

FIG. 2. Schematic of the experimental setup. Tritons are detected in the telescope and alpha particles are detected in the focal plane of the Enge split-pole spectrograph.

triton detectors, respectively) selectively samples a limited region of the breakup. These regions are indicated by the highlighted surface segments on the breakup spheres. They correspond to the backward and forward emissions of the breakup fragments in the primary scattered ^{7}Li reference frame. For the detector geometry shown, where the separation angle of the detectors, θ_{sep}^{det}, is less than the maximum separation angle of the emitted alpha particle and triton, θ_{sep}^{max}, the forward-backward solutions to sequential breakup are well separated in terms of the fragment laboratory energies, E_α and E_t, provided that the breakup is elastic.

The first excited state of ^{7}Li above breakup threshold is the 4.63-MeV $7/2^-$ state. Breakup from this state results in a well-defined relative energy of the alpha and triton of 2.16 MeV. By positioning the detectors such that $\theta_{sep}^{det} < \theta_{sep}^{max}$, breakup with $E_{rel}^{min} < E_{rel} < 2.16$ MeV can be detected, with the minimum energy E_{rel}^{min} determined by θ_I^{det}, the inner-edge separation angle between the detectors. These relative energies correspond to virtual excitations in the ^{7}Li and thus must represent direct breakup.

III. EXPERIMENTAL TECHNIQUE

The experiments were carried out using the upgraded MP Tandem Van de Graaff accelerator at the Nuclear Structure Research Laboratory. Beams of 54-MeV ^{7}Li were produced using a SNICS source and a LiOH cathode. The coincidence detection system consisted of a 200-μm Si ΔE, 5-mm Si(Li) E detector telescope for detecting tritons and a position-sensitive proportional counter [12], located in the focal plane of an Enge split-pole spectrograph [13], for detecting alpha particles. A schematic of the telescope-spectrograph detection system is shown in Fig. 2.

The telescope was mounted in the horizontal plane of the scattering chamber, thereby measuring breakup in the reaction plane (in-plane breakup). The telescope and spectrograph opening apertures were separated by a fixed $\theta_{sep}^{det} \simeq 12°$ (to be compared with $\theta_{sep}^{max} \simeq 23°$ for $E_{rel} = 2.16$ MeV) in order that alpha particles and tritons with relative energies down to 0.3 MeV (for $\theta_{sep} = \theta_{sep}^{det}$) could be detected while still probing very forward angles. For most measurements, the alpha particles were detected at smaller scattering angles than the tritons.

Aluminum absorber foils were placed in front of the telescopes to eliminate the elastically scattered beam. However, the E_t threshold due to these foils prohibited the detection of the backward-emitted tritons (corresponding to forward-emitted alpha particles) from sequential breakup of the $7/2^-$ state of ^{7}Li. In order to observe sequential breakup, the magnetic field in the spectrograph was chosen to transport backward-emitted alpha particles to the low-energy side of the proportional counter. (The high-energy E_α cutoff of the proportional counter was close to the low-energy E_t cutoff determined by the absorber foils, when considering elastic breakup. In addition, the magnetic rigidity of the elastically scattered ^{7}Li ions was too high to be detected at this field.) Data were normalized either to charge collected in a beam dump or to elastic-scattering rates in a monitor detector at 30°.

IV. RESULTS

The three-body kinematics for ^{7}Li breakup are governed by momentum conservation:

$$\mathbf{p}_\alpha + \mathbf{p}_t + \mathbf{p}_T = \mathbf{p}_{\text{Li}},$$

and reaction Q value:

$$E_\alpha + E_t + E_T = E_{\text{Li}} + Q,$$

where the subscripts Li and T represent the beam and target recoil, respectively. A plot of E_t vs E_α is shown

in Fig. 3 for 54-MeV ^{7}Li + ^{12}C in-plane breakup with $\theta_\alpha = 6°$ and $\theta_t = 18°$ ($\theta_{\rm lab} = 11°$), where the alpha particle and triton are detected in coincidence. A large fraction of breakup events fall on a locus of constant Q given by

$$Q_{ggg} = (m_{\rm Li} - m_\alpha - m_t)c^2 = -E_{\rm sep}$$

which corresponds to the fragments and target being left in their ground states. The locus appears straight because the variation of the target recoil energy is small over the range of fragment energies examined.

By projecting the events in Fig. 3 onto a summed-energy axis (indicated by the dashed line), peaks with well-defined Q values are formed. Typical $E_\alpha + E_t$ spectra for ^{7}Li + ^{12}C and ^{7}Li + ^{197}Au reactions are shown in Figs. 4(a) and 4(b), respectively. The highest-energy peak in Fig. 4(a) corresponds to elastic breakup. An additional peak corresponding to excitation of the 4.4-MeV 2^+ state of ^{12}C is also observed. In Fig. 4(b), the alpha-triton summed energy spectrum for ^{7}Li + ^{197}Au shows that the breakup is dominated by elastic and inelastic processes, with the lowest-lying states of ^{197}Au unresolved. This will be referred to as quasielastic breakup.

When probing the most-forward angles, additional peaks in the summed energy spectra were observed with both gold and carbon targets. Figure 5 shows such a spectrum for 54-MeV ^{7}Li + ^{12}C at $\theta_{\rm lab} \simeq 1°$. To obtain this lab angle, the spectrograph was positioned at $\theta_{\rm spec} = -4°$ with the telescope at $\theta_{sst} = 8°$. The elastic-breakup peak can be seen at $E_\alpha + E_t \simeq 52$ MeV. The broad peak centered around $\simeq 50$ MeV cannot result from excitation to a state, or a combination of states, of any nuclei in the exit channel [14]. Nor can this peak be attributed to transfer-induced breakup, such as ^{12}C(^{7}Li,^{8}Li* $\rightarrow \alpha tn$)^{11}C with $Q_{gggg} = -21$ MeV, since the summed-energy peak would shift to a much lower en-

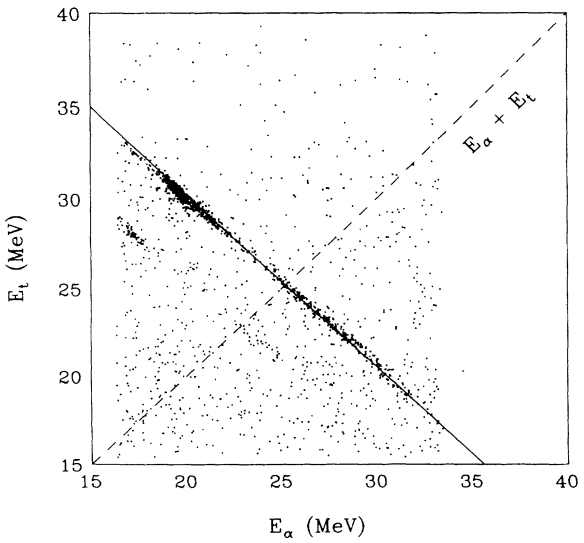

FIG. 3. E_α vs E_t spectrum for 54-MeV ^{7}Li + ^{12}C at $\theta_{\rm lab} = 11°$. The solid line corresponds to $Q = Q_{ggg}$. A summed-energy axis is indicated by the dashed line.

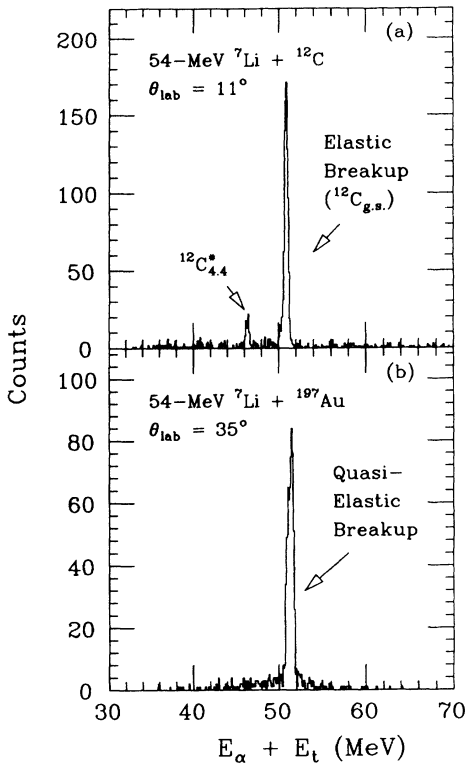

FIG. 4. $E_\alpha + E_t$ spectrum for (a) 54-MeV ^{7}Li + ^{12}C at $\theta_{\rm lab} = 11°$ and (b) 54-MeV ^{7}Li + ^{197}Au at $\theta_{\rm lab} = 35°$. The most energetic peak corresponds to elastic breakup (^{12}C) and quasielastic breakup (^{197}Au).

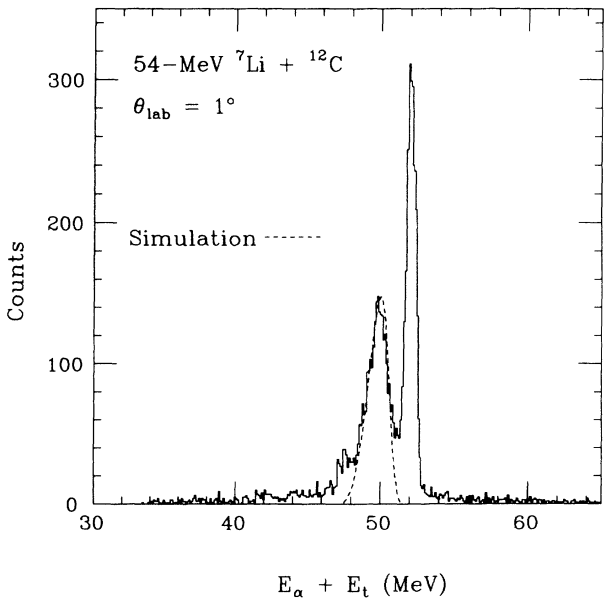

FIG. 5. $E_\alpha + E_t$ spectrum for 54-MeV ^{7}Li + ^{12}C at $\theta_{\rm lab} = 1°$. A broad peak is observed at ~ 50 MeV. The dashed curve is from a Monte Carlo simulation of 54-MeV ^{7}Li $+p$ elastic breakup (see text).

ergy. Since this peak is not observed at larger angles, it could result from ^{7}Li breakup on a light target contaminant, in which case the yield would be strongly forward focused. One possibility is hydrogen from hydrocarbons present in the scattering chamber, leading to $^7\mathrm{Li} + p$ reactions.

To investigate this, a Monte Carlo code was used to simulate sequential breakup, in which the emission of the alpha particle and triton is assumed to be isotropic in the ^{7}Li rest frame. The resulting $E_\alpha + E_t$ peak from $p(^7\mathrm{Li},^7\mathrm{Li}^*_{4.63} \rightarrow \alpha t)$ sequential breakup (convolved with detector resolution) is plotted with dashed lines in Fig. 5. The position and shape of the peak is in good agreement with the data.

Hydrocarbon contaminants in the ^{197}Au target also produce additional peaks in the $E_\alpha + E_t$ spectra generated from breakup reactions at forward angles. In this case, $^7\mathrm{Li} + {}^{12}\mathrm{C}$ reactions can be observed. Software acceptance gates were used to analyze elastic breakup on ^{12}C and quasielastic breakup on ^{197}Au. An estimate of the proton contribution to the breakup events in the acceptance gate from 54-MeV $^7\mathrm{Li} + {}^{12}\mathrm{C}$ at $\theta_{\mathrm{lab}} = 1°$ was $\approx 1\%$. The quasielastic gate on 54-MeV $^7\mathrm{Li} + {}^{197}\mathrm{Au}$ was free from $^7\mathrm{Li} + {}^{12}\mathrm{C}$ contributions at all angles studied.

Once elastic and quasielastic breakup are selected, the individual E_α (or E_t) spectrum identify the direct and sequential components of breakup. One such E_α spectrum is shown in Fig. 6 for 54-MeV $^7\mathrm{Li} + {}^{12}\mathrm{C}$ at $\theta_{\mathrm{lab}} = 11°$. A relative-energy axis is also shown, calculated assuming the alpha-triton separation angle to be the detectors' center-to-center separation angle, with $E_{\mathrm{rel}}^{\mathrm{min}} = 0.5$ MeV. (The minimum observable relative energy, corresponding to inner-edge detection, is 0.3 MeV.) The backward-emitted alpha particles from sequential breakup can be seen at $E_\alpha \simeq 20$ MeV. The sequential peak is kinematically broadened due to the angular acceptance of the detectors. The rest of the alpha events correspond to virtual excitations, and thus represent the direct breakup of ^{7}Li.

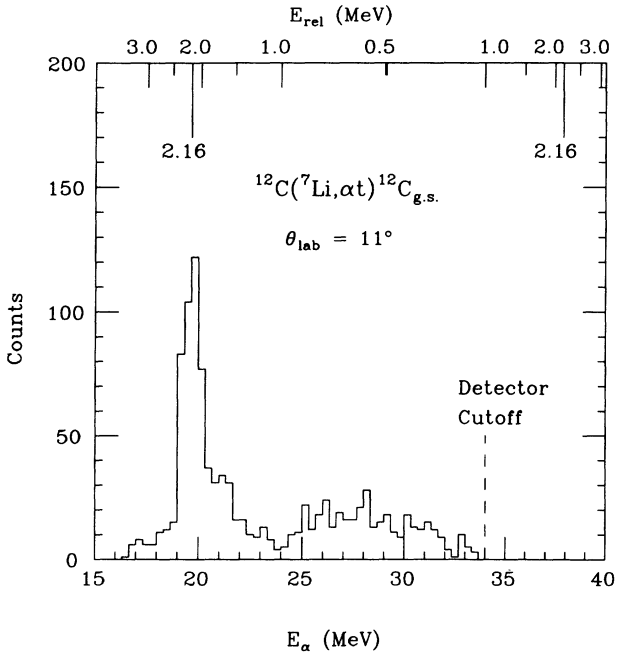

FIG. 6. Alpha energy spectrum for 54-MeV $^7\mathrm{Li} + {}^{12}\mathrm{C}$ at $\theta_{\mathrm{lab}} = 11°$, gated on elastic breakup. The sequential breakup peak is at $E_\alpha \sim 20$ MeV. Events with $E_\alpha > 20$ MeV are attributed to direct breakup. The high-energy detector cutoff is shown by the dashed line.

A. $^7\mathrm{Li} + {}^{12}\mathrm{C}$ direct-breakup yields

The direct-breakup yield was corrected for detector efficiency, which is a function of relative energy and, hence, a function of alpha energy. The detector efficiency was calculated using the sequential breakup simulation, in which the ^{7}Li is excited to a virtual state determined by

$$E^* = E_{\mathrm{rel}} + E_{\mathrm{sep}}.$$

The efficiency-corrected yield was summed over the observed alpha energies, excluding sequential breakup. The high-momentum cutoff prohibited detection of those forward-emitted alpha particles corresponding to large relative energies. These events were roughly accounted for by doubling the contribution from backward-emitted alpha particles of the same relative energies.

In an earlier analysis [11], yields were obtained by summing over the backward-emitted alpha particles and doubling the result to account for the forward-emitted alpha particles. Within experimental errors, the two approaches result in the same yields.

The direct-breakup differential cross sections for $^7\mathrm{Li} + {}^{12}\mathrm{C}$ are shown in Fig. 7, plotted as a function of the center-of-mass scattering angle of the primary ^{7}Li. (For direct breakup, the kinematics of the alpha-triton center of mass are equivalent to the kinematics of the scattered lithium.) Certain scattering angles were inaccessible us-

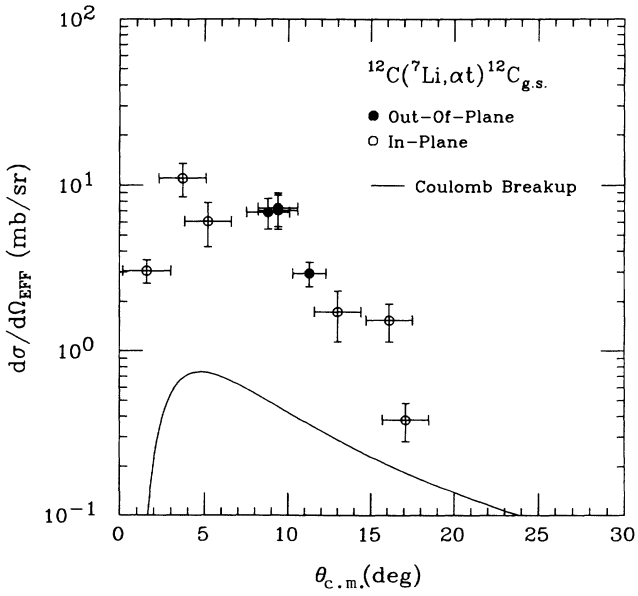

FIG. 7. Angular distribution for direct elastic breakup of $^7\mathrm{Li} + {}^{12}\mathrm{C}$. An $E1$ Coulomb breakup calculation is shown with a solid line (see text).

ing the in-plane detection system, due to blocking by the beam dump. Therefore, a second telescope was mounted 12.5° below the spectrograph opening—constituting an "out-of-plane" detector geometry—to probe these angles. (Note that this out-of-plane geometry examined angles between the breakup and reaction planes of 20°–43°, and thus is a weak measure of anisotropy.)

The measured yields are compared to a Coulomb-breakup calculation, in which the standard Coulomb-excitation formalism [15] is extended to virtual excitations. It has been shown that alpha-triton direct capture proceeds predominantly by electric dipole radiation through s-wave capture [16]. The Coulomb-breakup cross section is then given by

$$\frac{d\sigma}{d\Omega} = \int \left(\frac{Z_T e}{\hbar v_i}\right)^2 \frac{df_{E1}(\theta_{\text{c.m.}}, \xi)}{d\Omega} B(E1; E_{\text{rel}}) dE_{\text{rel}}, \tag{1}$$

with Z_T the target nuclear charge, v_i the initial relative velocity of the projectile and target in the entrance channel, $B(E1; E_{\text{rel}})$ the reduced matrix element for an $E1$ transition, and $df_{E1}(\theta_{\text{c.m.}}, \xi)/d\Omega$ the Coulomb excitation function. The symmetrized adiabaticity parameter is defined by

$$\xi = \frac{Z_P Z_T e^2}{\hbar} \left(\frac{1}{v_f} - \frac{1}{v_i}\right),$$

where Z_P is the projectile nuclear charge and v_f is the final relative velocity in the exit channel. In terms of the excitation energy,

$$v_f = \sqrt{\frac{2}{m_{\text{Li}}} \left[E_{\text{Li}} - \left(1 + \frac{m_P}{m_T}\right) E^*\right]},$$

where m_T is the target mass. The $B(E1; E_{\text{rel}})$ values were computed using data from radiative capture measurements [16] using detailed balance arguments [2]. The Coulomb excitation functions were calculated semiclassically using standard techniques [15].

The solid line in Fig. 7 represents a Coulomb-breakup calculation obtained from Eq. (1), integrated over the relative energy range measured experimentally. As can be seen, the experimental cross sections at forward angles are significantly larger than the calculated Coulomb-breakup yields. This lack of agreement indicates a large contribution to the direct-breakup yield from the target nuclear field. (The importance of nuclear forces on breakup has previously been observed using another loosely bound projectile, the deuteron, in reactions with a ^{12}C target [17].) In order to extract direct-capture cross sections from direct breakup using detailed balance, direct breakup must be well described by a first-order Coulomb process. Therefore, the direct breakup measured with the ^{12}C target is not suitable for extracting astrophysical S factors.

Recently, it was suggested [4] that a "universal" relative-energy dependence of the breakup cross sections (due to a "parallelism" between nuclear and Coulomb excitations) may be used to extract direct-capture cross sections when there are nuclear components in the breakup. However, further theoretical studies [7] have shown that the spectrum of virtual excitations is quite different for Coulomb and nuclear breakup—especially at the lowest E_{rel}.

B. ^{7}Li + ^{197}Au direct breakup

The distribution of forward-emitted and backward-emitted alpha particles should be roughly symmetric about the single-value solution where the minimum detectable relative energy ($E_{\text{rel}}^{\text{min}}$) is observed, corresponding to equal fragment laboratory velocities. In the case of 54-MeV ^{7}Li + ^{197}Au at $\theta_{\text{lab}} = 19°$, $E_\alpha(E_{\text{rel}}^{\text{min}}) \approx 29.6$ MeV. However, for the results shown in Fig. 8, the observed spectrum is very asymmetric about this $E_\alpha(E_{\text{rel}}^{\text{min}})$. There is, in fact, an apparent depletion in yield of low-energy alpha particles from direct breakup. Such a behavior is not observed in the fragment energy spectra of ^{7}Li + ^{12}C.

The question of post-breakup acceleration of the breakup fragments due to the Coulomb repulsion of the target has previously been raised for these reactions [3, 18, 19]. Such final-state interactions would have the effect of shifting the asymptotic energies of the breakup fragments due to their different q/m. This differential Coulomb acceleration would also alter their asymptotic relative energies.

One can make a simple estimate of this effect in terms of the Coulomb interaction of the projectile and fragments with the target. Assuming the breakup occurs at a distance d from the target, the fragment-target Coulomb potential is then calculated for each fragment. This results in an energy boost for the alpha particle of

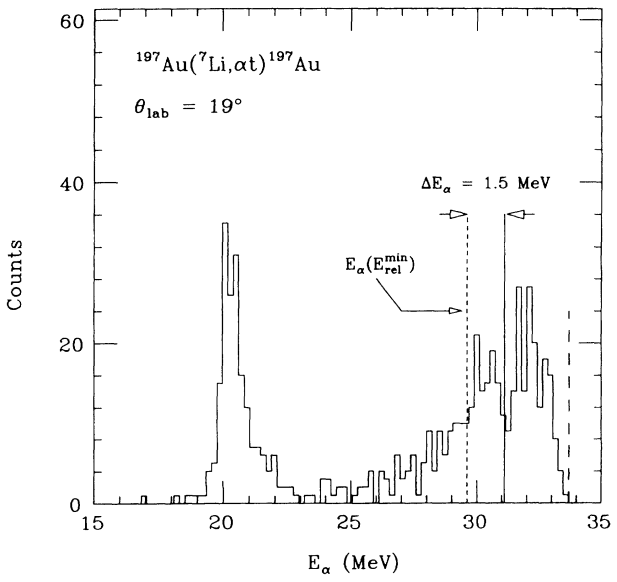

FIG. 8. Alpha energy spectrum for 54-MeV ^{7}Li + ^{197}Au at $\theta_{\text{lab}} = 19°$. The short-dashed line indicates the value of E_α corresponding to $E_{\text{rel}}^{\text{min}}$. The solid line represents the shift in the asymptotic energy of the alpha particle, $E_\alpha(E_{\text{rel}}^{\text{min}}) + \Delta E_\alpha$, as calculated in the text.

$$\Delta E_\alpha = \left(\frac{Z_\alpha}{m_\alpha} - \frac{Z_{\rm Li}}{m_{\rm Li}}\right)\frac{m_\alpha Z_T e^2}{d}. \quad (2)$$

The triton experiences an equal and opposite shift in energy.

For sequential breakup via the $7/2^-$ state, the long lifetime of the state ($\tau \simeq 10^{-20}$ s) leads to dissociation far from the target, where these final-state interactions are weak. Direct breakup, on the other hand, due to its prompt nature, occurs closer to the target, and these energy shifts cannot be ignored. If the breakup is assumed to occur at the classical distance of closest approach, then the alpha energy shift as calculated by Eq. (2) is $\Delta E_\alpha = 1.5$ MeV at $\theta_{\rm lab} = 20°$, in qualitative agreement with observation (Fig. 8).

As is illustrated schematically in Fig. 1, different detector arrangements selectively sample breakup events from different regions of the breakup spheres. For breakup near the gold target, this sampling might be influenced by target-proximity effects. To investigate this further, the orientation of the detectors was reversed so that the tritons were detected at more-forward angles than the alpha particles.

This comparison was made for 54-MeV ^{7}Li + ^{197}Au, with "in-plane" detector angles of $\theta_\alpha = 14°$ and $\theta_t = 26.5°$, and "reversed"-geometry angles of $\theta_\alpha = 24.8°$ and $\theta_t = 12.3°$. These detector angles correspond to the same laboratory scattering angle of 19.4° for the primary ^{7}Li.

The alpha energy spectra for in-plane and reversed-geometry measurements are shown in Figs. 9(a) and 9(b), respectively. The asymmetry seen in Fig. 8 is again observed in Fig. 9(a), but the direct E_α distribution in Fig. 9(b) exhibits a small shift in energy, opposite in direction to that observed with in-plane geometry. The depletion of the sequential breakup at $E_\alpha \sim 20$ MeV in Fig. 9(b) is a reflection of the collection time, since the sequential breakup yield is insensitive to this reversal of detector geometry. If one scales the spectra of Figs. 9(a) and 9(b) by their sequential breakup peaks, one observes a fivefold increase in the direct-breakup yield measured with reversed geometry as compared to in-plane geometry.

The simple energy-shift calculation, which is independent of detector geometry, fails to explain these results. Therefore, a more realistic modeling of the breakup reaction, including proximity effects, was undertaken.

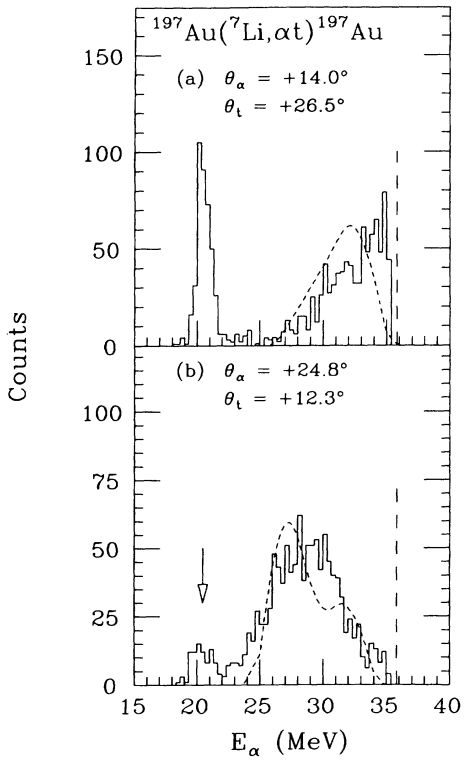

FIG. 9. Alpha energy spectrum for 54-MeV ^{7}Li + ^{197}Au at $\theta_{\rm lab} = 19.4°$. (a) In-plane detector geometry. (b) Reversed detector geometry. The dashed lines are from simulations that include post-breakup interactions (see text). The arrow indicates the sequential breakup from the $7/2^-$ state in ^{7}Li.

C. Three-body trajectory calculations

A simulation was developed to calculate three-body classical Coulomb trajectories in order to take fragment orientation and fragment-fragment interactions into account. This simulation made the following assumptions: (1) the particles follow Coulomb trajectories, (2) breakup occurs at the distance of closest approach, and (3) at the point of breakup, the ^{7}Li is treated as an extended object.

For $E1$ breakup of 54-MeV ^{7}Li + ^{197}Au with $\theta_{\rm lab} = 19.4°$, the relative-energy distribution [determined by the integrand of Eq. (1) and shown in Fig. 10] has a maximum at ~ 0.6 MeV. Therefore, the simulation was performed using a single value of $E_{\rm rel} = 0.6$ MeV.

Both ^{7}Li and target follow Coulomb trajectories until

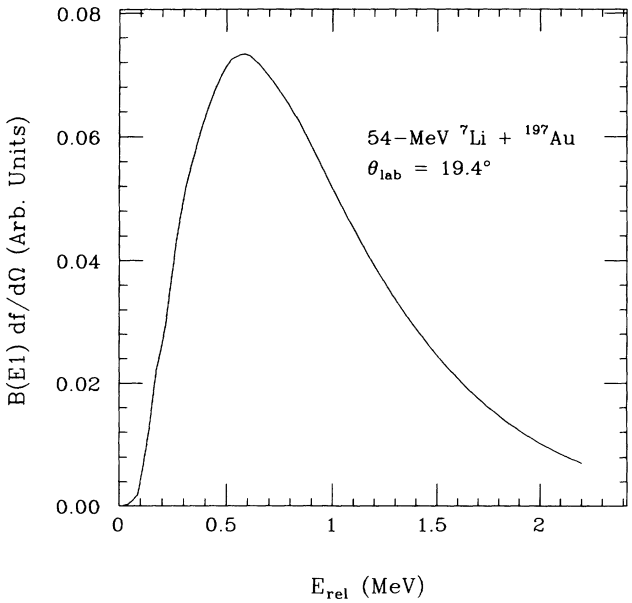

FIG. 10. $E_{\rm rel}$ distribution for 54-MeV ^{7}Li + ^{197}Au at $\theta_{\rm lab} = 19.4°$ calculated assuming $E1$ Coulomb excitation. The yield is peaked at ~ 0.6 MeV.

they arrive at the distance of closest approach (d=23.2 fm for θ_{lab} = 19.4°). At this point, the ^{7}Li is treated as an extended object. An alpha-triton separation of 4.8 fm is used, corresponding to a mutual Coulomb interaction of 0.6 MeV. In the absence of any further target interaction, this separation will result in an asymptotic value of E_{rel} = 0.6 MeV. The trajectories of the breakup fragments are then calculated, subject to the target-fragment and fragment-fragment Coulomb repulsions, until asymptotic values are obtained.

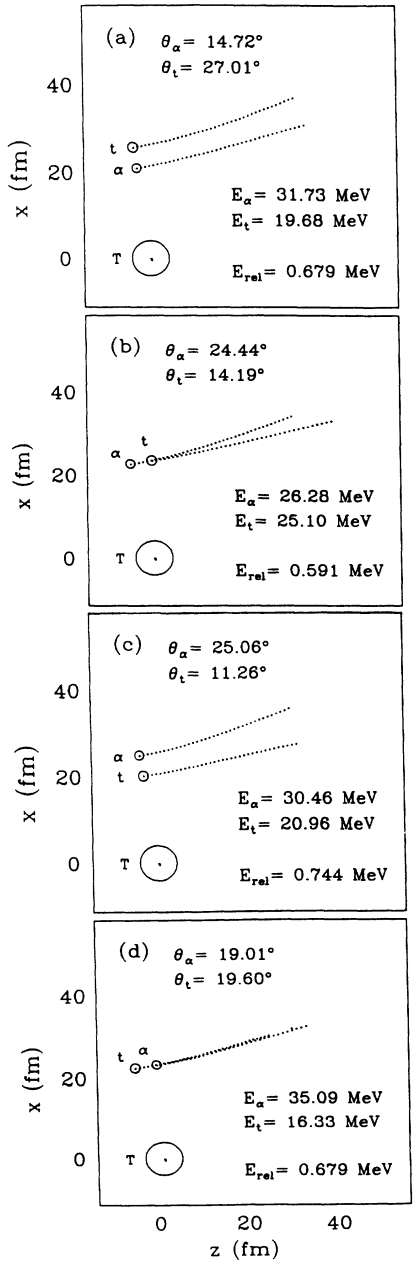

FIG. 11. Fragment Coulomb trajectories for 54-MeV ^{7}Li + ^{197}Au at θ_{lab} = 19.4° for various breakup orientations with respect to the target. Breakup occurs at the distance of closest approach, d = 23.2 fm, with a *local* relative energy of E_{rel} = 0.6 MeV. Asymptotic fragment energies and scattering angles are indicated, as well as *asymptotic* relative energies.

To illustrate the effects of treating the ^{7}Li as an extended object, the trajectories of the nuclei in the exit channel, calculated using four different in-plane orientations of the fragments at the time of breakup, are shown in Fig. 11. In Fig. 11(a), the alpha particle and triton are separated perpendicular to the trajectory of the ^{7}Li, with the alpha particle emitted closer to the target. This orientation is then rotated successively by $\pi/2$, about the alpha-triton center of mass, to generate Figs. 11(b), 11(c), and 11(d). The asymptotic energies and angles of the fragments are shown in the figure for the four orientations. As can be seen, each orientation results in different values of the asymptotic relative energy. This distortion of the relative energy is a reflection of final-state interactions with the target.

In order to compare the results of this simulation to the experimental yields, the trajectories were calculated for all orientations of the breakup fragments, chosen randomly. The asymptotic angles at which the breakup fragments were emitted were then compared to the angular regions subtended by the detectors to determine coincidence events.

Figure 12 shows the location of the alpha particle in the ^{7}Li frame, at the time of breakup. The x-z plane

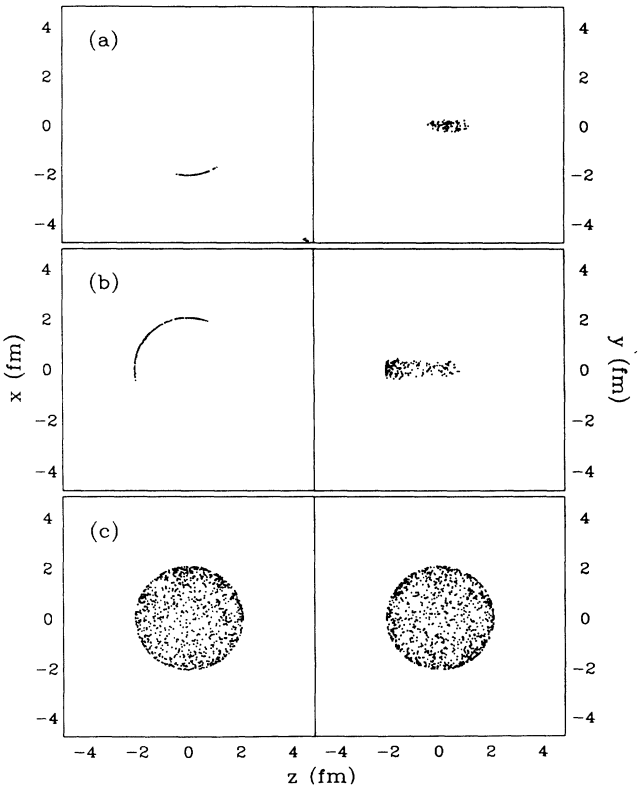

FIG. 12. Alpha particle breakup spheres for 54-MeV ^{7}Li + ^{197}Au at θ_{lab} = 19.4°. The x-z plane is the horizontal plane, with z along the beam direction. The location of the alpha particle at the time of breakup is plotted with respect to the ^{7}Li for a coincidence measurement with (a) in-plane geometry and (b) reversed geometry. For comparison, isotropic emission of alpha particles is shown in (c).

is the horizontal plane, with the beam in the $+z$ direction. The isotropic emission of the breakup fragments is illustrated in Fig. 12(c). The in-plane and reversed geometries select different regions of the breakup spheres, as shown in Figs. 12(a) and 12(b), respectively. As can be seen, a larger range of breakup orientations can be detected with the reversed geometry, which is therefore more efficient for detecting direct breakup. In fact, the simulation reproduces the factor of ~ 5 increase in detector efficiency for the reversed geometry, as compared to the in-plane measurement.

The resulting alpha energy spectra from the classical-trajectory simulations for both in-plane and reversed geometries are shown in Figs. 9(a) and 9(b), respectively, as dashed curves. The simulated spectrum for in-plane geometry was scaled to the measured yield, with the scaling for reversed geometry then determined by the calculated detector efficiencies. The simulation qualitatively reproduces the experimental distributions for the two different detector geometries. It should be noted that the distributions generated by the simulation are sensitive to the separation distance between the breakup fragments.

Recently, asymmetries in angular correlations have been observed in 60-MeV ^{6}Li $\rightarrow \alpha + d$ breakup [19], for which the q/m differential acceleration is negligible. The measurements were performed forward of grazing on a high-Z target (^{208}Pb) and nuclear contributions were not observed. The observed asymmetries could not be reproduced by first-order Coulomb breakup, but rather were attributed by the authors to final-state interactions.

Applying the three-body trajectory calculations (described above) to ^{6}Li, in which the projectile is treated as an extended object at breakup, we observe that target-proximity effects distort the asymptotic relative energies of the breakup fragments. The simulations were conducted assuming a fixed local $E_{\rm rel}$ of 600 keV, an isotropic distribution of breakup orientations, and a fixed α-d opening angle of 12°. As was the case for ^{7}Li, the coincidence efficiency is strongly modulated by detector geometry. In particular, the efficiency is found to vary by a factor of ≈ 3 as the out-of-plane angle, ϕ_a, varies (using the notation of [19]). These simulations indicate that fragment q/m ratios alone are not sufficient for evaluating final-state Coulomb effects.

D. ^{7}Li + ^{197}Au direct-breakup yields

The efficiency correction used to extract yields on the ^{12}C target was generated using a sequential-like calculation, which, by its very nature, neglects target-proximity effects. For data on ^{197}Au, such effects are clearly evident, and, in fact, severely complicate the extraction of breakup cross sections, since the efficiency is no longer a function of just $E_{\rm rel}$ (or E_α), but now contains a strong dependence on detector orientation. Therefore, in order to calculate the experimental cross sections, the classical-trajectory simulation was used to generate the efficiency. Since the simulated and measured E_α distributions have similar shapes, the efficiency correction described earlier can be reduced to a simple scaling.

The direct-breakup cross sections for ^{7}Li + ^{197}Au are

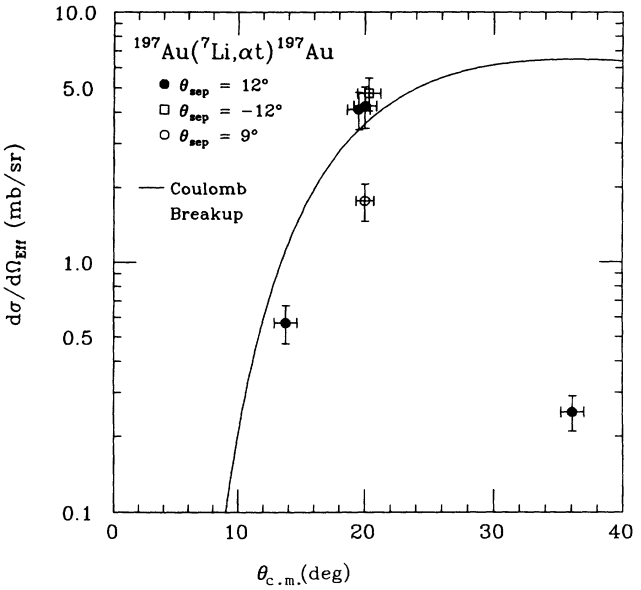

FIG. 13. Angular distribution for direct quasielastic breakup of ^{7}Li + ^{197}Au. An $E1$ Coulomb breakup calculation is shown with a solid line (see text).

shown in Fig. 13. The solid line in Fig. 13 is the result of an $E1$ Coulomb-breakup calculation (described earlier). The experimental cross sections are approximately reproduced, within a factor of 2, by the Coulomb-breakup calculation, except at the most-backward angle. (This backward angle is near the grazing angle calculated using an *effective* interaction radius for the breakup fragments and the target, where $r_0 = 1.4$ fm and the alpha-triton separation is included. Therefore, the decreased yield is most likely due to nuclear absorption—especially for the in-plane geometry used.)

Agreement at the forward angles suggests that direct breakup at these angles results from a Coulomb process. However, to calculate S factors, one needs the *local* relative energy distribution (associated with the spectrum of virtual excitation), as deduced from the measured asymptotic distribution. To account for the final-state interactions requires knowledge of where the breakup occurred and what orientation the alpha particle and triton had with respect to the target. However, even by imposing geometric constraints on the detection system, a broad region of the breakup spheres is sampled. As a result, a given value of the asymptotic $E_{\rm rel}$ is found to arise from a convolution of local $E_{\rm rel}$ and breakup-orientation distributions. Consequently, there is no unique mapping from asymptotic to local values of the relative kinetic energy.

In contrast to these conclusions, another study of ^{7}Li breakup [3, 4] cited yield minima at $E_{\rm rel} = 0$ MeV (unshifted by Coulomb effects) as evidence that the breakup took place far from the target. This was supported by the long lifetime inferred from the width of the direct-breakup continuum [3]. However, the stability of relative-energy minima can also arise from the alpha-triton interaction, and thus is not a good measure of final-state

interactions with the target. Furthermore, the width of the $E_{\rm rel}$ continuum is determined by transmission coefficients and virtual photon spectra (the latter a reflection of reaction kinematics), and thus cannot be analyzed as a long-lived resonance [8].

V. CONCLUSIONS

Direct breakup of ^{7}Li is observed on both ^{12}C and ^{197}Au targets. For ^{7}Li + ^{12}C elastic breakup, calculated Coulomb-breakup cross sections substantially underpredict the experimental yields, implying a strong nuclear component in the reaction. For ^{7}Li + ^{197}Au quasielastic breakup, the calculated Coulomb-breakup cross sections qualitatively agree with the data at the forward angles. Even though direct breakup appears to result from a Coulomb process at these angles, orientation effects and final-state interactions are found to distort the energy spectra and modulate detector efficiency. Such effects prohibit one from accurately determining astrophysical S factors.

More work is required to determine optimum experimental conditions for using direct breakup to probe radiative capture. Future experiments on ^{7}Li + ^{197}Au will investigate the kinematic and geometric conditions under which the post-breakup interactions and orientation effects are minimized. Simulations show that these effects can be greatly suppressed by going to more forward angles, corresponding to larger distances of closest approach. However, the direct-breakup yield diminishes rapidly as the interaction becomes weaker, and thus a more efficient detection system will be required.

ACKNOWLEDGMENTS

We would like to thank the operations staff at NSRL for providing excellent ^{7}Li beams. We also thank F. L. H. Wolfs for a critical reading of the manuscript. This work was supported by the National Science Foundation under Grant No. PHY-8920580. One of us (S.B.G.) acknowledges the financial support of the NSF Presidential Young Investigator Program.

[1] A. C. Shotter, A. N. Bice, J. M. Wouters, W. D. Rae, and J. Cerny, Phys. Rev. Lett. **46**, 12 (1981).
[2] A. C. Shotter, V. Rapp, T. Davison, D. Branford, N. E. Sanderson, and M. A. Nagarajan, Phys. Rev. Lett. **53**, 1539 (1984).
[3] H. Utsunomiya, R. P. Schmitt, Y. W. Lui, D. R. Haenni, H. Dejbakhsh, L. Cooke, P. Heimberg, A. Ray, W. Turmel, and T. Udagawa, Phys. Lett. B **211**, 24 (1989).
[4] H. Utsunomiya, Y. W. Lui, D. R. Haenni, H. Dejbakhsh, L. Cooke, B. K. Srivastava, W. Turmel, D. O'Kelly, R. P. Schmitt, D. Shapira, J. Gomez del Campo, A. Ray, and T. Udagawa, Phys. Rev. Lett. **65**, 847 (1990).
[5] I. J. Thompson and M. A. Nagarajan, Phys. Lett. **123B**, 379 (1983).
[6] C. A. Bertulani and M. S. Hussein, Nucl. Phys. **A524**, 306 (1991).
[7] R. Shyam, G. Baur, and P. Banerjee, Phys. Rev. C **44**, 1253 (1991).
[8] D. K. Srivastava, D. N. Basu, and H. Rebel, Phys. Lett. B **206**, 391 (1988).
[9] H. Rebel, Workshop on Nuclear Reaction Cross Sections of Astrophysical Interest (Kernforschungszentrum Karlsrule Report, 1985, unpublished).
[10] G. Baur, C. A. Bertulani, and H. Rebel, Nucl. Phys. **A458**, 188 (1986).
[11] S. B. Gazes, J. E. Mason, R. B. Roberts, and S. G. Teichmann, Phys. Rev. Lett. **68**, 150 (1992)
[12] H. W. Fulbright, R. G. Markham, and W. A. Lanford, Nucl. Instrum. Methods **108**, 125 (1973).
[13] J. E. Spencer and H. A. Enge, Nucl. Instrum. Methods **49**, 181 (1967).
[14] S. Fiarman and W. E. Meyerhof, Nucl. Phys. **A206**, 1 (1973); S. Fiarman and S. S. Hanna, *ibid.* **A251**, 1 (1975); F. Ajzenberg-Selove, *ibid.* **A433**, 1 (1985).
[15] K. Alder, A. Bohr, T. Huus, B. Mottleson, and A. Winther, Rev. Mod. Phys. **28**, 432 (1956).
[16] G. M. Griffiths, R. A. Morrow, P. J. Riley, and J. B. Warren, Can. J. Phys. **39**, 1397 (1961).
[17] E. C. May, B. L. Cohen, and T. M. O'Keefe, Phys. Rev. **164**, 1235 (1967).
[18] G. Baur and M. Weber, Nucl. Phys. **A405**, 352 (1989).
[19] J. Hesselbarth and K. T. Knöpfle, Phys. Rev. Lett. **67**, 2773 (1991); J. Hesselbarth, S. Khan, Th. Kihm, and K. T. Knöpfle, Z. Phys. A **331**, 365 (1988).